

Hybrid optimization for high-precision parameter extraction in Mo/Au/AlGa_N/Ga_N Schottky diodes

M. Mostefaoui^a, A. Rabehi^b, A. Hatem Kacha^c, K. Hammouche^c, H. Mazari^c,
K. Ameer^c, J.-M. Bluet^d, A. Douara^e, A. Rabehi^{b,c}, and M. Benganem^f

^a*Department of Preparatory Classes, Higher School of Saharan Agriculture, Adrar 01000, Algeria,*

^b*Laboratory of Telecommunications and Smart Systems, Faculty of Sciences and Technologies,
University of Djelfa, Djelfa 17000, Algeria,*

^c*Applied Microelectronics Laboratory, Department of Electronics, Djillali Liabes University of Sidi Bel Abbes,
BP 89, 22000, Sidi Bel Abbes, Algeria,*

^d*Université de Lyon, Institut des Nanotechnologies de Lyon INL-UMR5270, CNRS, INSA de Lyon,
Villeurbanne F-69621, France,*

^e*Faculty of Science and Technology, Tissemsilt University, Tissemsilt, 38000, Algeria,*

^f*Physics Department, Faculty of Science, Islamic University of Madinah, Madinah, 42351, Saudi Arabia.*

Received 1 April 2025; accepted 29 July 2025

Accurate parameter extraction is essential for understanding and optimizing the performance of Mo/AlGa_N/Ga_N Schottky barrier diodes (SBDs). Traditional methods often introduce approximation errors, particularly in the presence of high series resistance. In this study, we propose a hybrid approach that combines Nonlinear Least Squares Fitting (NLSF) with the Lambert W function and Grey Wolf Optimization (GWO) to achieve high-precision extraction of key diode parameters, including the ideality factor n , barrier height (ϕ_b), and series resistance (R_s). By leveraging the strengths of both analytical and metaheuristic techniques, this method enhances accuracy and robustness in parameter estimation. Experimental validation across a wide temperature range (100 K - 450 K) demonstrates the effectiveness of the proposed approach, highlighting its advantages over conventional extraction techniques.

Keywords: Schottky barrier diode; AlGa_N/Ga_N; parameter extraction; grey wolf optimization; Lambert W function; temperature dependence.

DOI: <https://doi.org/10.31349/RevMexFis.72.011601>

1. Introduction

Gallium Nitride (Ga_N) and its related materials have attracted considerable attention due to their exceptional properties, making them highly suitable for high-power, high-frequency, and high-temperature applications. One of the most significant advancements in this field is the heteroepitaxial growth of Ga_N on silicon (Si) substrates, which serves as a critical foundation for the development of a wide range of high-performance electronic devices [1].

Compared to conventional silicon Si and gallium arsenide (GaAs) devices, Ga_N-based semiconductors offer significant advantages, including a wide bandgap, high breakdown voltage, and superior electron mobility [2–6]. Among these materials, AlGa_N/Ga_N heterostructures are particularly promising for the development of advanced semiconductor devices, such as high-electron-mobility transistors (HEMTs) used in next-generation RF and microwave power amplifiers for wireless communication systems [7–13].

The performance of AlGa_N/Ga_N HEMTs is strongly influenced by the choice of substrate material. Commonly used substrates include sapphire, silicon (Si), and silicon carbide (SiC) [14–18].

While sapphire is cost-effective, its poor thermal conductivity limits heat dissipation, negatively impacting device efficiency [19–24].

On the other hand, SiC substrates, although more expensive, provide superior crystal quality and excellent thermal conductivity, making them the preferred choice for high-performance power devices. The AlGa_N/Ga_N heterostructure exhibits a two-dimensional electron gas (2DEG) at the heterointerface due to the combined effects of spontaneous and piezoelectric polarization [25]. This 2DEG, characterized by an electron mobility of approximately 2000 cm²V⁻¹s, plays a crucial role in enabling high-speed and high-power operation [26].

A critical parameter affecting the performance of these devices is the Schottky barrier height (SBH) of the gate electrode. A higher SBH leads to reduced leakage currents and improved breakdown voltage, thereby enhancing both the noise performance and power efficiency of HEMTs [27]. At metal-semiconductor interfaces, the SBH in Ga_N and AlGa_N materials shows a stronger dependence on the metal work function compared to other III-V semiconductors, indicating weaker Fermi level pinning and greater tunability of the barrier height [28].

However, Schottky diodes formed on Ga_N and AlGa_N materials exhibit excess reverse leakage currents that significantly exceed the predictions of the standard thermionic emission (TE) model [29]. Despite this, many studies continue to analyze their current-voltage I-V characteristics

using the TE model, highlighting the need for improved parameter extraction techniques [30].

In this study, we focus on the precise extraction of key electrical parameters, including the barrier height ϕ_{bn} , ideality factor n , series resistance R_s , and parallel resistance R_p , by analyzing forward bias I-V characteristics in the temperature range of 100-450 K. To achieve accurate parameter estimation, we compare three different techniques: the traditional method based on standard I-V curve fitting, Nonlinear Least Squares Fitting (NLSF), and Grey Wolf Optimization (GWO). The traditional technique relies on analytical aligns and linear approximations, while NLSF refines parameter estimation by minimizing the sum of squared residuals between the model and experimental data. In contrast, GWO is a nature-inspired optimization algorithm that enhances accuracy by efficiently exploring the solution space [31–33]. By comparing these methods, we aim to assess their strengths and limitations, ultimately identifying the most reliable approach for extracting Schottky diode parameters.

2. Experimental details

The studied structure was grown using Low-Pressure Metal Organic Chemical Vapor Deposition (LP-MOCVD) on a SiC substrate. Nucleation occurs through an intermediate layer, followed by the deposition of an unintentionally doped GaN buffer layer with a thickness of 1.7 μm . The ohmic contacts consist of a titanium (12 nm), aluminum (200 nm), nickel (40 nm), and gold (100 nm) stack, deposited by electron-beam evaporation and subsequently annealed at 900°C for 30 seconds under a nitrogen atmosphere. Component isolation is achieved through helium ion implantation, followed by annealing under a nitrogen atmosphere. The Schottky gate contacts are composed of a bilayer of molybdenum (40 nm) and gold (300 nm), deposited by electron-beam evaporation. Component passivation is achieved by sequentially depositing a 100 nm SiO₂ dielectric layer, followed by a 50 nm Si₃N₄ layer. The buffer layer, sufficiently thick, acts as a substrate for the upper layers. On top of this, an Al_{0.28}Ga_{0.72}N layer is deposited with a defined thickness for this structure, remaining unintentionally doped.

The aluminum mole fraction x in the Al_{*x*}Ga_{1-*x*}N barrier layer was estimated using Vegard's law, which assumes a linear relationship between the lattice constant and the alloy composition. Based on the X-ray diffraction (XRD) measurements of the (002) reflection, the c-lattice constants of GaN and Al_{*x*}Ga_{1-*x*}N layers were found to be 5.180 Å and 5.122 Å, respectively. Using the known lattice constant of AlN (4.970 Å), the mole fraction x is calculated using the formula [30]:

$$x = \frac{c_{\text{GaN}} - c_{\text{AlGaN}}}{c_{\text{GaN}} - c_{\text{AlN}}} = \frac{5.180 - 5.122}{5.180 - 4.970} \approx 0.28. \quad (1)$$

Figure 1 illustrates the architecture of the studied HEMT structure and an electron microscope image.

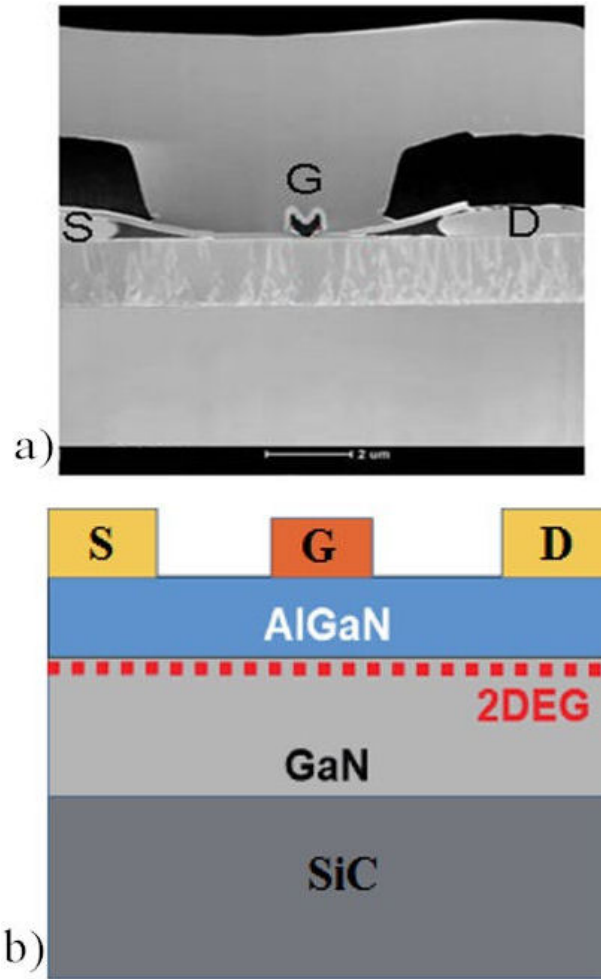


FIGURE 1. a) Architecture of the studied HEMT structure, b) electron microscope image of a HEMT transistor.

The experimental measurements on Al_{0.28}Ga_{0.72}N/GaN structures were conducted at the Institute of Nanotechnology of Lyon, INSA Lyon, using a specialized setup to analyze $I_g(V_{gs})$ behavior as a function of temperature (see Fig. 2). The system includes a liquid nitrogen cryostat (TRG model, TBT, Groupe Air Liquide) for cooling the sample within a temperature range of 77 K to 500 K, ensuring a stable low-temperature environment. A temperature controller (LTC-11) precisely regulates the sample temperature by controlling the cryostat's heating and cooling systems. Electrical measurements are performed using an HP 4156 A semiconductor parameter analyzer, which applies gate-source and gate-drain voltage biases while measuring the resulting gate current (I_g) under cryogenic conditions. The sample is placed inside the cryostat, which includes a 25 ohm heating resistor for temperature regulation. This setup enables precise electrical characterization of Al_{0.28}Ga_{0.72}N/GaN structures over a wide temperature range, providing valuable insights into their electrical properties and thermal behavior. The semi-logarithmic forward-bias I-V-T characteristics of (Mo/Au)-AlGa_{*x*}N/GaN HEMTs at various temperatures are illustrated in Fig. 3.

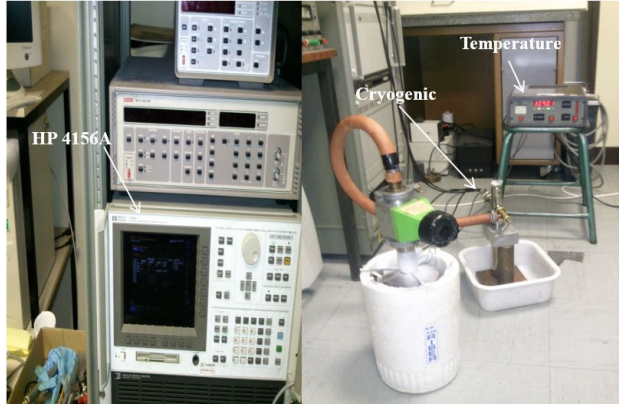


FIGURE 2. Experimental setup for electrical characterization of AlGaN/GaN HEMTs under cryogenic conditions.

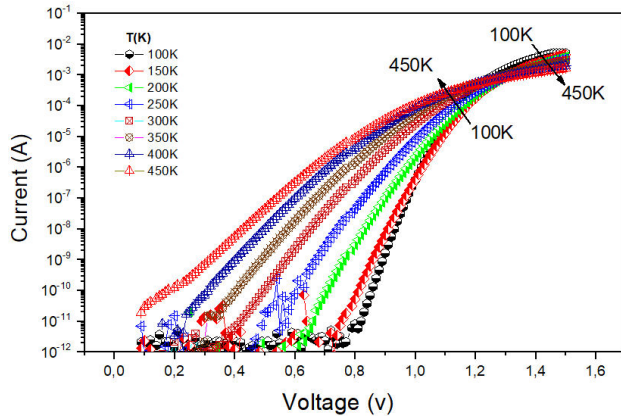


FIGURE 3. Forward and reverse bias semilogarithmic I-V characteristics of a (Mo/Au)-AlGaN/GaN HEMTs at various temperatures.

2.1. Polarization-Induced 2DEG and temperature dependence

The analysis of the capacitance-voltage (C-V) characteristics allows for the experimental determination of the electron density n_s in the two-dimensional electron gas (2DEG). To validate the presence of the 2DEG, capacitance measurements were performed between the gate and the source of the device at a frequency of 1 MHz (Fig. 4).

The carrier density n_s of the 2DEG is calculated using the following align [30]:

$$n_s = \int \frac{C_{2DEG} dv}{qS} \quad (V : 0 - V_{th}), \quad (2)$$

where C_{2DEG} is the 2DEG capacitance. V_{th} is the threshold voltage, q is the elementary charge (1.6×10^{-19} C), S is the gate area (3.75×10^{-5} cm²),

From the C-V curve, the measured capacitance is approximately 9.98 pF, and the threshold voltage is $V_{th} = -6.11$ V. Substituting these values into the align yields a 2DEG carrier density of:

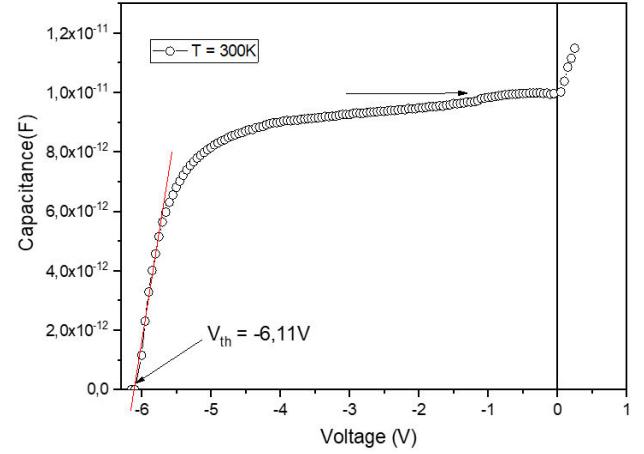


FIGURE 4. Experimental C-V characteristics of (Mo/Au)-Al_{0.28}Ga_{0.72}N/GaN HEMTs at $T = 300$ K.

$$n_s \approx \frac{9.98 \times 10^{-12} \cdot 6.11}{1.6 \times 10^{-19} \cdot 3.75 \times 10^{-5}} \approx 1.02 \times 10^{13} \text{ cm}^{-2}, \quad (3)$$

This result confirms the formation of a two-dimensional electron gas at the AlGaN/GaN interface. The 2DEG sheet density at the Al_xGa_{1-x}N heterointerface arises due to the spontaneous and piezoelectric polarization discontinuities. For the estimated Al mole fraction $x = 0.28$, the polarization difference ΔP can be expressed as [30]:

$$\begin{aligned} \Delta P &= P_{\text{AlGaN}} - P_{\text{GaN}} \approx P_{\text{SP}} - P_{\text{PZ}} \\ &\approx -0.052 + 0.026 = -0.026 \text{ C/m}^2, \end{aligned} \quad (4)$$

Assuming full charge transfer and no compensation, the estimated 2DEG sheet density is:

$$n_s = \frac{|\Delta P|}{e} \approx \frac{0.026}{1.6 \times 10^{-19}} \approx 1.6 \times 10^{13} \text{ cm}^{-2}. \quad (5)$$

The behavior of the two-dimensional electron gas (2DEG) at the Al_{0.28}Ga_{0.72}N/GaN interface exhibits a strong dependence on temperature and aluminum content. At low temperatures (100-200 K), carrier freeze-out in the barrier layer or at trap states can lead to a reduction in carrier mobility and overall current conduction. However, due to the polarization-induced nature of the 2DEG, it generally remains populated even at cryogenic temperatures, maintaining a baseline conductivity. As the temperature increases beyond 300 K, phonon scattering becomes the dominant mobility-limiting mechanism, resulting in performance degradation. Additionally, the Al mole fraction plays a critical role in shaping the 2DEG characteristics. A higher Al content enhances the spontaneous and piezoelectric polarization fields, which increases the 2DEG sheet density (n_s) by deepening the quantum well at the heterointerface. This interplay between temperature effects and polarization strength is essential to understanding the nonlinearity observed in the current-voltage characteristics at elevated temperatures and higher current densities.

3. The description of the SBD model

For the ideal SBD, it is assumed that the forward bias current of the device is due to the thermionic emission current and can be expressed as [34–36]:

$$I_{TE} = I_s \left[\exp \left(q \frac{V - R_S I_{TE}}{nkT} \right) \right], \quad (6)$$

where I_s is the saturation current, and given by [13, 36]:

$$I_s = SA^*T^2 \exp \left(\frac{-q\phi_{bn}}{kT} \right), \quad (7)$$

where q is the electron charge, bn is the barrier height, R_S is the series resistance, n the ideality factor, k is the Boltzmann constant, S is the effective diode area and T is the temperature in Kelvin, A^* is the effective Richardson constant.

The effective Richardson constant is a material-dependent parameter that characterizes electron emission over a potential barrier. It is defined by the following align:

$$A^* = \frac{4\pi q m^* k^2}{h^3}, \quad (8)$$

where h is Planck's constant and m^* is the effective mass of the electron in the semiconductor.

The ideality factor n , ϕ_{bn} Schottky barrier height bn , and series resistance R_S are the characteristic parameters of the SBDs and should be determined as accurately as possible from experimental $I(V)$ characteristics.

4. Methods for optimal estimation of schottky diode parameters

In this study, we compared three different methods for parameter estimation of the Schottky diode: the traditional technique, Nonlinear Least Squares Fitting (NLSF), and Grey Wolf Optimization (GWO). Each method offers distinct advantages and limitations in extracting key diode parameters such as n , ϕ_{bn} and R_S .

TABLE I. Comparison of extracted parameters using different methods.

T (K)	Method	ϕ_{bn} (eV)	n	R_s (Ω)
100	Analytical method	0.536	2.57	30.30
	NLSF-Lambert W	0.541	2.55	29.80
	GWO	0.540	2.56	29.90
150	Analytical method	0.623	2.36	48.78
	NLSF-Lambert W	0.627	2.34	48.10
	GWO	0.625	2.35	48.40
200	Analytical method	0.801	2.14	55.55
	NLSF-Lambert W	0.805	2.12	54.90
	GWO	0.803	2.13	55.00
250	Analytical method	0.990	1.39	76.92
	NLSF-Lambert W	0.995	1.37	76.20
	GWO	0.993	1.38	76.50
300	Analytical method	1.060	1.28	87.00
	NLSF-Lambert W	1.065	1.26	86.20
	GWO	1.063	1.27	86.50
350	Analytical method	1.150	1.18	105.20
	NLSF-Lambert W	1.153	1.16	104.80
	GWO	1.152	1.17	105.00
400	Analytical method	1.210	1.144	133.30
	NLSF-Lambert W	1.215	1.140	132.50
	GWO	1.213	1.142	132.80
450	Analytical method	1.250	1.07	153.80
	NLSF-Lambert W	1.253	1.06	153.10
	GWO	1.252	1.065	153.40

4.1. Analytical method (The semi-logarithmic ($\ln I - V$) plot method)

The semi-logarithmic ($\ln I - V$) plot method is a traditional technique used to extract key Schottky diode parameters, such as n , b_n and R_S , from I-V characteristics. This method is based on the thermionic emission model Eq. (1), which describes the diode current behavior mathematically. While effective, it can introduce approximation errors, especially in the presence of high series resistance. The ideality factor can be gained by the slope of $\ln I$ versus voltage plot, if this slope is inserted in align:

$$n = \frac{q}{kt} \left(\frac{dv}{d \ln I} \right). \quad (9)$$

To extract the barrier height, align 2 transforms into:

$$\phi_{bn} = \frac{kT}{q} \ln \left(\frac{SA^* T^2}{I_s} \right). \quad (10)$$

The obtained values of ϕ_{bn} , n and R_S as a function of temperature are shown in Table I.

4.2. Nonlinear least squares fitting (NLSF) with Lambert W function

The Lambert W function is a powerful mathematical tool used for solving aligns where the unknown variable appears both inside and outside an exponent, making it particularly useful for modeling the I-V characteristics of Schottky diodes. In this study, we apply Nonlinear Least Squares Fitting (NLSF) with the Lambert W function to optimize the extraction of electrical parameters, including the barrier height (ϕ_{bn}), ideality factor (n), and series resistance (R_S).

4.2.1. Mathematical formulation

First, the thermionic current terms are combined together:

$$I_S \exp \left(\frac{qV}{nkT} \right) = I_{TE} \exp \left(\frac{qR_S I_{TE}}{nkT} \right). \quad (11)$$

By defining a new variable:

$$w = \frac{qR_S I_{TE}}{nkT}. \quad (12)$$

We rewrite the align as:

$$w \exp(w) = \left(\frac{qR_S}{nkT} \right) I_S \exp \left(\frac{qV}{nkT} \right). \quad (13)$$

Applying the Lambert W function:

$$w = W_0 \left[\left(\frac{qR_S}{nkT} \right) I_S \exp \left(\frac{qV}{nkT} \right) \right]. \quad (14)$$

Thus, the current is expressed as:

$$I_{TE} = \frac{nkT}{qR_S} W_0 \left[\left(\frac{qR_S}{nkT} \right) I_S \exp \left(\frac{qV}{nkT} \right) \right]. \quad (15)$$

4.2.2. Optimization Using NLSF

To determine the optimal values of ϕ_{bn} , n , and R_S , the model parameters are fitted to experimental I-V data using Nonlinear Least Squares Fitting (NLSF). The objective function is to minimize the Root Mean Square Error (RMSE) between the experimental and theoretical currents:

$$e = \sqrt{\frac{1}{L} \sum_{j=1}^L [I_{\text{exp}}(V_j) - I_{\text{model}}(V_j, \theta)]^2}, \quad (16)$$

where $I_{\text{exp}}(V_j)$ represents the measured current at voltage, $I_{\text{model}}(V_j, \theta)$ represents the fitted model current, and $\theta = [\phi_{bn}, n, R_S]$ is the set of parameters to be estimated.

The Levenberg-Marquardt algorithm is typically employed for minimizing, ensuring fast convergence while handling nonlinearities in the model. The obtained values of ϕ_{bn} , n and R_S as a function of temperature are shown in Table I.

4.3. Grey wolf optimization (GWO)

Grey Wolf Optimization (GWO) is a nature-inspired metaheuristic algorithm that mimics the social hierarchy and hunting behavior of grey wolves. First introduced by Mirjalili *et al.*, GWO has been widely applied in solving complex optimization problems, including parameter estimation for electronic devices like Schottky Barrier Diodes (SBDs).

Unlike traditional numerical methods, GWO does not require derivative information and efficiently handles nonlinear systems, making it a robust approach for extracting key electrical parameters (ϕ_{bn} , n , and R_S).

4.3.1. Mathematical formulation

The estimation of Schottky diode parameters follows a structured approach, beginning with the collection of experimental I-V data. The Grey Wolf Optimizer (GWO) is then applied to optimize the parameters (ϕ_{bn} , n , and R_S), ensuring precise alignment with empirical measurements.

Since Eq. (1) follows a highly nonlinear relationship, it is transformed into a more computationally efficient form to facilitate parameter estimation. The modified align is expressed as:

$$y(I, V, \theta) = I - I_0 [\exp(q(V - IR_S)/nkT) - 1] = f(I, V, \theta), \quad (17)$$

where $\theta = [\phi_{bn}, n, \text{ and } R_S]$ represents the unknown parameters. To obtain optimal values, the Root Mean Square Error (RMSE) is minimized:

$$e = \sqrt{\frac{1}{L} \sum_{j=1}^L [y(I_j, V_j, \theta)]^2}. \quad (18)$$

By employing GWO, the algorithm iteratively adjusts θ to reduce e , leading to an accurate and computationally efficient estimation of Schottky diode parameters.

TABLE II. GWO algorithm parameters.

Parameter	Value
Population Size	20
Number of Iterations	1000
Search Agents	20
Convergence Factor	Decreasing linearly from 2 to 0
Lower Bound $[n, R_s, \varphi_{bn}]$	[1, 10, 0.4]
Upper Bound $[n, R_s, \varphi_{bn}]$	[3, 200, 1.2]
Alpha (α)	Best solution
Beta (β)	Second best solution
Delta (δ)	Third best solution
Omega (ω)	Remaining search agents

4.3.2. GWO Algorithm Implementation

The GWO algorithm is structured in three main phases:

A. Encircling the Prey (Exploration Phase).

Wolves adjust their positions dynamically based on the best solution (\vec{X}_p):

$$\vec{D} = \left| \vec{C} \cdot \vec{X}_p - \vec{X} \right|,$$

$$\vec{X}_{new} = \vec{X}_p - \vec{A} \cdot \vec{D}, \quad (19)$$

where \vec{X} = Position of the wolf (solution), \vec{X}_p = Best solution found so far (prey), \vec{A}, \vec{C} = Coefficient vectors controlling movement, defined as: with \vec{r}_1, \vec{r}_2 , as random values in $[0, 1]$, and \vec{a} a linearly decreases from 2 to 0.

B. Hunting (Exploitation Phase).

The top three best solutions guide the optimization process:

$$\vec{X}_{new} = \frac{\vec{X}_\alpha + \vec{X}_\beta + \vec{X}_\delta}{3}, \quad (20)$$

where $X_\alpha, X_\beta, X_\delta$ are the three best solutions at each iteration. The distances from these leaders are calculated as:

$$\vec{D}_\alpha = \left| \vec{C}_1 \cdot \vec{X}_\alpha - \vec{X} \right|$$

$$\vec{D}_\beta = \left| \vec{C}_2 \cdot \vec{X}_\beta - \vec{X} \right| \quad (21)$$

$$\vec{D}_\delta = \left| \vec{C}_3 \cdot \vec{X}_\delta - \vec{X} \right|$$

These aligns adjust each wolf's movement based on the leading wolves.

C. Attacking the Prey (Convergence Phase).

As iterations progress, wolves reduce exploration and converge on the optimal solution. This is controlled by

$$\vec{a} = 2 - \frac{2t}{T}, \quad (22)$$

where t = Current iteration, T = Maximum iterations.

When $|\vec{A}| < 1$, wolves focus on exploitation, ensuring convergence (solution is found). The GWO Algorithm Parameters are shown in Table II and the obtained values of $\Phi_b n$, n and R_S as a function of temperature are shown in Table I.

5. Results and discussion

As shown in Fig. 1, the forward bias I-V characteristics are linear in the intermediate bias regions, but when the applied bias voltage is sufficiently large it started deviate considerably from linearity this is due the R_S effect. The variation of R_S with temperature exhibits an unusual behavior, increasing as the temperature rises, as illustrated in Fig. 4b). This behavior generally contradicts the commonly observed negative temperature coefficient of R_S . The increase in R_S at low temperatures is attributed to the limited availability of free charge carriers in the absence of carrier freezing out, which becomes significant only at low temperatures [37–39]. According to Osvald and Horvath [38], the series resistance rises sharply at low temperatures due to the scarcity of free charge carriers. As the temperature increases, the thermal generation of charge carriers (electrons or holes) in the semiconductor is enhanced under both positive and negative bias conditions. Similar temperature dependence of R_S has been observed in both experimental [37] and theoretical studies [38].

From Table I, it can be observed that the NLSF-Lambert W method estimates the lowest R_S values, demonstrating its accuracy in correcting for voltage drop effects. The GWO method produces slightly higher values but remains close to the NLSF results, confirming its robustness in optimizing resistance parameters. In contrast, analytical method yield the highest R_S values, underscoring their limitations in accounting for non-idealities in experimental I-V data.

We can also observe from Table I that the barrier height ($\Phi_b n$) increases with temperature, which aligns with theoretical expectations due to temperature-dependent Schottky barrier formation. Among the three methods, NLSF-Lambert W consistently provides the highest barrier height values, indicating a more precise parameter extraction technique. GWO yields slightly lower values but remains very close to NLSF, confirming its efficiency in approximating accurate parameters. Analytical method, however, tend to underestimate $\Phi_b n$, which is likely due to the approximations inherent in stepwise calculations.

As illustrated in Fig. 4b) and observed from Table II, the ideality factor n values decrease with increasing temperature, which suggests a reduction in charge carrier recombination and tunneling effects as the thermal energy increases. NLSF-

TABLE III. Comparative evaluation of parameter estimation methods.

Criterion	Analytical Method	NLSF with Lambert W	GWO
Accuracy	Moderate (higher errors at low temperatures)	High (best match with experimental data)	Moderate-High (close to NLSF but slightly less precise)
Computational Complexity	Low (fast but requires multiple assumptions)	High (requires solving nonlinear aligns iteratively)	Moderate (requires multiple iterations but efficient in global search)
Robustness	Low (sensitive to noise and high series resistance)	High (handles variations well, less sensitive to noise)	High (global search capability reduces effect of noise and variations)

Lambert W results in the lowest values of n , indicating that it captures the ideal diode behavior more effectively.

GWO also provides close estimates but tends to be slightly higher, while analytical method consistently overestimates n , especially at lower temperatures. This overestimation may be attributed to the influence of series resistance and the sensitivity of analytical techniques to measurement noise. From these observations, it is evident that NLSF with the Lambert W function is the most precise method for extracting diode parameters, as it provides the most refined estimates for $\Phi_b n$, n , and R_S . GWO, while slightly less accurate than NLSF, remains a highly effective alternative, particularly useful when no initial parameter estimates are available. On the other hand, analytical method tend to introduce greater errors, particularly at lower temperatures, where their approximations become less reliable. However, at higher temperatures (300 – 450 K), all three methods produce more convergent results, suggesting that non-ideal effects are more pronounced at lower temperatures. To further compare these methods based on additional performance metrics, Table III presents an evaluation based on accuracy, computational complexity, and robustness.

This comparative analysis highlights that NLSF with Lambert W function is the most precise method, offering the best accuracy and robustness but requiring significant computational effort. GWO presents a strong alternative, striking a balance between accuracy and computational efficiency, making it suitable when initial parameter values are unknown. In contrast, analytical method, while computationally fast, introduce higher errors and are more sensitive to data variations, making them less reliable for precise modeling. Overall, NLSF with Lambert W is recommended for high-precision parameter extraction, while GWO serves as an effective alternative for cases requiring global optimization. Analytical method remain useful for quick estimates but show significant limitations in handling non-idealities.

5.1. Leakage current analysis at 300 K

Figure 5 illustrates the gate leakage current (I_g) versus gate-source voltage (V_{gs}) measured at 300 K for the (Mo/Au)/Al_{0.28}Ga_{0.72}N/GaN Schottky diode. The I-V curve is presented on a logarithmic scale, revealing an ex-

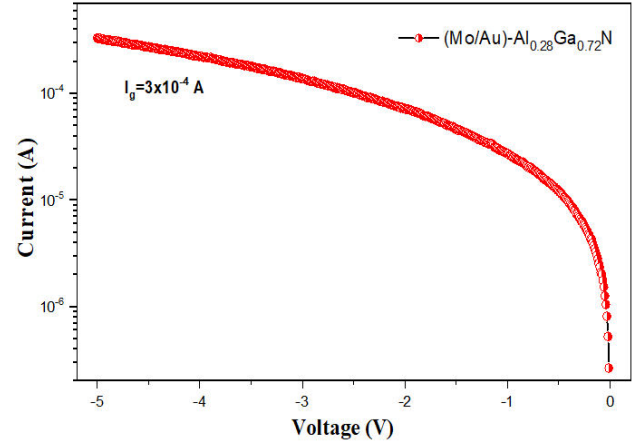


FIGURE 5. Shows the gate leakage current I_g as a function of the gate-source voltage V_{gs} under reverse bias conditions.

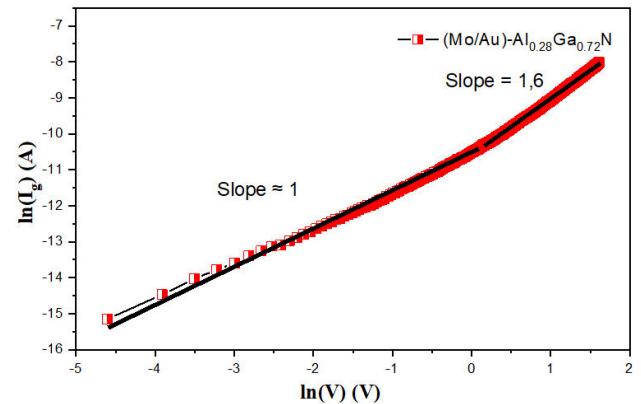


FIGURE 6. The transformation $\ln(I_g)$ vs $\ln(V)$ for the current I_g as a function of the gate-source voltage V_{gs} under reverse bias conditions.

ponential decay of leakage current under increasing reverse bias.

In reverse bias, various models can be employed to fit the obtained I-V curve, indicating the presence of multiple current transport mechanisms. To identify these mechanisms and extract the relevant model parameters, logarithmic transformations were applied to highlight linear regions within the fitted curve. The first mechanism observed in the reverse bias region corresponds to ohmic conduction, as evidenced by the plot $\ln(I_g)$ of $\ln(V)$ shown in Fig. 6. This plot reveals two

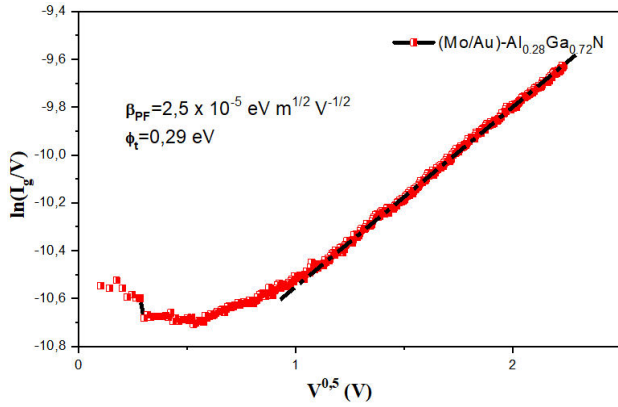


FIGURE 7. The transformation \ln for the current I_g as a function of the gate-source voltage V_{gs} under reverse bias conditions.

distinct linear regions, each characterized by a different slope. The initial slope is approximately 1, which is consistent with ohmic behavior [30]. The second slope, however, is around 1.6, deviating from the initial linear regime. This suggests the involvement of a different conduction mechanism, potentially space charge limited conduction (SCLC), which is typically characterized by a theoretical slope of 2 [30].

The second mechanism fitting the reverse curve is for Poole-Frenkel emission, using the transformation $\ln(I_g/V)$ vs \sqrt{V} plotted in Fig. 7.

The model for the Poole-Frenkel type emission is given by [30]:

$$I_{PFE} \propto \exp\left(-\frac{\Phi_t}{k_b T}\right) \exp\left(\frac{\beta_{PF} \sqrt{V}}{k_b T d^{1/2}}\right), \quad (23)$$

where Φ_t is the emission barrier height for trap state and β_{PF} is the Poole-Frenkel emission coefficient.

$$\beta_{PF} = \left(\frac{q^3}{\pi \epsilon_0 \epsilon}\right)^{1/2}. \quad (24)$$

The calculated values of β_{PF} and Φ_t are ($2.5 \times 10^{-5} \text{ eV m}^{-1/2} \text{ V}^{1/2}$) and 0.29 eV. Besides, the relative permittivity calculated is 9.22 for (Mo/Au)/Al_{0.28}Ga_{0.72}N.

6. Conclusion

This study compares three parameter estimation methods: Analytical, Nonlinear Least Squares Fitting (NLSF) with the Lambert W function, and Grey Wolf Optimization (GWO) for Mo/Au/AlGa_{0.28}N/GaN Schottky diodes. Among these, the NLSF with the Lambert W function method proves to be the most accurate, effectively minimizing non-linear effects and providing precise extraction of key parameters (Φ_{bn} , n , and R_s). However, it demands higher computational resources. GWO offers a robust and efficient alternative, especially for complex models, although it slightly underperforms compared to NLSF in terms of precision. The analytical method,

while fast and simple, tends to introduce errors at lower temperatures due to its reliance on approximations.

The results indicate that the barrier height Φ_{bn} increases with temperature, while the ideality factor n decreases, reflecting reduced recombination and tunneling effects. The series resistance R_s shows an unusual increase with temperature, attributed to carrier freeze-out at lower temperatures.

Overall, NLSF with the Lambert W function is recommended for applications requiring high accuracy, while GWO serves as a viable alternative when initial estimates are unavailable. The analytical method remains useful for quick estimations despite its limitations. Future work could explore hybrid approaches combining GWO's global search capabilities with NLSF's local refinement to further enhance parameter extraction efficiency and accuracy.

The gate leakage current behavior of the (Mo/Au)/Al_{0.28}Ga_{0.72}N Schottky diode was thoroughly investigated at 300 K. The analysis revealed the presence of multiple transport mechanisms under reverse bias. Initially, ohmic conduction was identified at low voltages, followed by a transition toward space-charge limited conduction (SCLC) as the applied bias increased. Furthermore, Poole-Frenkel emission was found to dominate at higher electric fields, indicating the role of trap-assisted conduction in the dielectric. These findings contribute to a better understanding of leakage current behavior in AlGa_{0.28}N/GaN-based Schottky structures and highlight the influence of material properties on device performance.

Funding

This research did not receive any external funding.

Data availability

The datasets used and/or analyzed during the current study are available from co-author Prof. Abdelaziz Rabehi (*rab_ehi@hotmail.fr*) on reasonable request.

Author Contributions Statement Data availability

Conceptualization, M.M., A.R. (Abdelhalim Rabehi), and A.H.K.; methodology, M.M., A.H.K., A.D., and A.R. (Abdelaziz Rabehi); software, A.R. (Abdelaziz Rabehi) and M.G.; validation, A.R. (Abdelhalim Rabehi), A.D., and J.-M.B.; formal analysis, A.R. (Abdelaziz Rabehi), M.G., and M.B.; investigation, H.M., K.A., and J.-M.B.; resources, A.D., J.-M.B., and M.B.; data curation, M.M., A.R. (Abdelhalim Rabehi), H.M., K.A., and M.G.; writing-original draft preparation, A.R. (Abdelaziz Rabehi), M.M., and M.B.; writing-review and editing, A.R. (Abdelaziz Rabehi), M.G., A.H.K., and J.-M.B.; visualization, A.R. (Abdelaziz Rabehi), M.G., and A.D.; supervision, A.R. (Abdelhalim Rabehi), M.M., and M.B.; project administration, M.M., A.R. (Abdelhalim Rabehi), and A.R. (Abdelaziz Rabehi). All authors have read and agreed to the published version of the manuscript.

Acknowledgements

The researchers wish to extend their sincere gratitude to the Deanship of Scientific Research at the Islamic University

of Madinah (KSA) for the support provided to the Post-Publishing Program.

1. Z. Tekeli, Ş. Altındal, M. Çakmak, S. Özçelik, D. Çalişkan, and E. Özbay, The behavior of the I-V-T characteristics of inhomogeneous (NiAu) - Al 0.3Ga0.7 NAlNGaN heterostructures at high temperatures, *J Appl Phys*, **102** (2007) 1, <https://doi.org/10.1063/1.2777881>
2. A. Rabehi *et al.*, Accurate parameter estimation of Au/GaN/GaAs schottky diode model using grey wolf optimization, *Rev. Mex. Fis.* **70** (2024) 1, doi: <https://doi.org/10.31349/RevMexFis.70.021004>
3. A. Douara, A. Rabehi, O. Baitiche, and M. Hamdani, Improved electrical characteristics of Al_x Ga_{1-x}N/GaN High Electron Mobility Transistor by effect of physical and geometrical parameters, *Rev. Mex. Fis.* **69** (2023) doi: <https://doi.org/10.31349/RevMexFis.69.041001>
4. A. Rabehi, A. Douara, M. Elbar, R. Zenzen, and M. Amrani, Impact Of Grain Boundaries On The Electrical Characteristics And Breakdown Behavior Of Polycrystalline Silicon Pin Diodes: A Simulation Study, *Journal of Engineering and Technology for Industrial Applications*, **10** (2024) 59, <https://doi.org/10.5935/jetia.v10i49.1196>
5. A. Douara, A. Rabehi, M. Guermoui, R. Daha, and I. E. Tibermacine, Simulation-based optimization of barrier and spacer layers in InAlN/GaN HEMTs for improved 2DEG density, *Micro and Nanostructures*, **195** (2024), <https://doi.org/10.1016/j.micrna.2024.207950>
6. C. Wang, S. J. Cho, and W. S. Lee, A novel method for the fabrication of AlGaIn / GaN HEMTs on Si (111) substrates, (2012), <https://doi.org/10.1007/s00170-012-4583-4>
7. A. Rabehi *et al.*, Current-Voltage, Capacitance-Voltage-Temperature, and DLTS Studies of Ni—6H-SiC Schottky Diode, *Semiconductors*, **55** (2021) 446, <https://doi.org/10.1134/S1063782621040138>
8. A. Ziane *et al.*, Frequency Dependent Capacitance and Conductance-Voltage Characteristics of Nitride GaAs Schottky Diode, *Semiconductors*, **55** (2021) 51, <https://doi.org/10.1134/S1063782621010206>
9. A. Ziane *et al.*, Numerical investigation of G-V measurements of metal - A nitride GaAs junction, *Rev. Mex. Fis.* **70** (2024) 1, doi: <https://doi.org/10.31349/RevMexFis.70.061604>
10. H. Helal *et al.*, A new approach to studying the electrical behavior and the inhomogeneities of the Schottky barrier height, *Eur Phys J Plus*, **137** (2022) <https://doi.org/10.1140/epjp/s13360-022-02672-0>
11. F. Mekaret *et al.*, A comparative study of Schottky barrier heights and charge transport mechanisms in 3C, 4H, and 6H silicon carbide polytypes, *AIP Adv*, **14** (2024) <https://doi.org/10.1063/5.0240123>
12. H. Helal *et al.*, Conduction mechanisms in au/0.8 nm-gan/n-gaas schottky contacts in a wide temperature range, *Materials*, **14** (2021) <https://doi.org/10.3390/ma14205909>
13. M. J. Legodi, W. E. Meyer, and F. D. Auret, Interface properties of an O₂ annealed Au / Ni / n - Al 0. 18 Ga 0. 82 N Schottky contact, *Physica B: Physics of Condensed Matter*, **407** (2012) 1599, <https://doi.org/10.1016/j.physb.2011.09.095>
14. A. Douara, A. Rabehi, and O. Baitiche, Impact of AlN interlayer on the electronic and I-V characteristics of In_{0.17}Al_{0.83}N/GaN HEMTs devices, *Rev. Mex. Fis.* **69** (2023) 031602, <https://doi.org/10.31349/RevMexFis.69.031602>
15. A. Douara, A. Rabehi, and M. Hamdani, Effect of Geometrical and Physical parameters of AlGaIn/GaN HEMT on the electrical characteristics with AlN spacer layer, (2022).
16. A. Douara, A. Rabehi, M. Guermoui, R. Daha, and I. E. Tibermacine, Impact of AlN Buffer Layer Thickness on Electronic and Electrical Characteristics of In_{0.17}Al_{0.83}N/GaN High- Electron-Mobility Transistor, *Physics of the Solid State*, **66** (2024) 157, <https://doi.org/10.1134/S1063783424600766>
17. A. Rabehi *et al.*, Modeling the Abnormal Behavior of the 6H-SiC Schottky Diode Using Lambert W Function, *Journal of Nano- and Electronic Physics*, **14** (2022), [https://doi.org/10.21272/JNEP.14\(6\).06032](https://doi.org/10.21272/JNEP.14(6).06032)
18. E. Arslan, Tunneling current via dislocations in Schottky diodes on AlInN/AlN/GaN heterostructures, **075003** (2009) 075003, <https://doi.org/10.1088/0268-1242/24/7/075003>
19. A. Rabehi, H. Helal, D. Zappa, and E. Comini, Advancements and Prospects of Electronic Nose in Various Applications: A Comprehensive Review, **01** (2024), Multidisciplinary Digital Publishing Institute (MDPI). <https://doi.org/10.3390/app14114506>
20. M. W. Bouabdelli, F. Rogti, M. Maache, and A. Rabehi, Performance enhancement of CIGS thin-film solar cell, *Optik (Stuttg)*, **216** (2020), doi: 10.1016/j.ijleo.2020.164948.
21. H. Helal, M. Ahrouch, A. Rabehi, D. Zappa, and E. Comini, Nanostructured Materials for Enhanced Performance of Solid Oxide Fuel Cells: A Comprehensive Review, **01** (2024) Multidisciplinary Digital Publishing Institute (MDPI). <https://doi.org/10.3390/cryst14040306>
22. O. Baitiche, F. Bendelala, A. Cheknane, A. Rabehi, and E. Comini, Numerical Modeling of Hybrid Solar/Thermal Conversion Efficiency Enhanced by Metamaterial Light Scattering for Ultrathin PbS QDs-STPV Cell, *Crystals (Basel)*, **14** (2024) <https://doi.org/10.3390/cryst14070668>

23. A. M. Younsi, A. Rabehi, L. Gacem, and M. T. Soltani, Ab-initio study on structural, magnetic, electronic and optical properties of SrCo_{1-x}A_xO₃ (A = Fe or Cr, x = 0.125 and 0.25), *Modern Physics Letters B*, **38** (2024) <https://doi.org/10.1142/S0217984924500556>
24. M. Mostefaoui *et al.*, Anomalous behavior of forward I-V and C-V characteristics of Schottky gate AlGa_N/Ga_N HEMTs, *Journal of Optoelectronics and Advanced Materials*, **16** (2014).
25. S. Milazzo *et al.*, Applied Surface Science Tunneling and thermionic emission as charge transport mechanisms in W-based Schottky contacts on AlGa_N/Ga_N heterostructures, **679** (2025).
26. J. Yang, X. Zhang, and C. Lv, Study on the reliability of AlGa_N/Ga_N HEMTs at high temperature, 2011 International Conference on Electric Information and Control Engineering, *ICEICE 2011 - Proceedings*, **774** (2011) <https://doi.org/10.1109/ICEICE.2011.5777464>
27. J. Kotani, file:D:/4. H. 3/AlGa_N. mohamed/Nouveau dossier/1-s2. 0-S. pdfHideki Hasegawa, and T. Hashizume, Computer simulation of current transport in Ga_N and AlGa_N Schottky diodes based on thin surface barrier model, *Appl Surf Sci*, **237** (2004) 213, <https://doi.org/10.1016/j.apsusc.2004.06.152>
28. M. M. O. Ambacher, a) J. Smart, J. R. Shealy, N. G. Weimann, K. Chu and and L. F. E. W. J. Schaff, Two-dimensional electron gases induced by spontaneous and piezoelectric polarization charges in N- and Ga-face AlGa_NGa_N heterostructures, *J Appl Phys*, **85** (1999) 308, <https://doi.org/10.1007/BF00458847>
29. W. S. Lau, J. B. H. Tan, and B. P. Singh, Formation of Ohmic contacts in AlGa_N/Ga_N HEMT structures at 500° by Ohmic contact recess etching, *Microelectronics Reliability*, **49** (2009) 558, <https://doi.org/10.1016/j.microrel.2009.02.010>
30. H. Helal, Z. Benamara, M. Ben Arbia, A. Rabehi, A. C. Chaouche, and H. Maaref, Electrical behavior of n-GaAs based Schottky diode for different contacts: Temperature dependence of current-voltage, *International Journal of Numerical Modelling: Electronic Networks, Devices and Fields*, **34** (2916) 2021, <https://doi.org/10.1002/jnm.2916>
31. A. Rabehi *et al.*, Optimal estimation of Schottky diode parameters using a novel optimization algorithm: Equilibrium optimizer, *Superlattices Microstruct*, **146** (2020) <https://doi.org/10.1016/j.spmi.2020.106665>
32. A. Rabehi *et al.*, Optimal Estimation of Schottky Diode Parameters Using Advanced Swarm Intelligence Algorithms, *Semiconductors*, **54** (2020) 1398, <https://doi.org/10.1134/S1063782620110214>
33. Q. Li and Y. Zhang, Atomic-column resolution quantitative composition analysis of Al_N interlayer in MOCVD-grown AlGa_N/Al_N/Ga_N heterostructure using HAADF-STEM, *AIP Adv.*, **13** (2023) 1, <https://doi.org/10.1063/5.0123768>
34. I. Nifa *et al.*, Characterization and modeling of 2DEG mobility in AlGa_N/Al_N/Ga_N MIS-HEMT, *Microelectron. Eng.* **215** (2019) 110976, <https://doi.org/10.1016/j.mee.2019.05.003>
35. A. Carlotto *et al.*, Study of trapping mechanisms affecting AlGa_N/Ga_N HEMTs adopting AlGa_N back-barriers with different aluminum concentrations, *Microelectron. Reliab.* **170** (2025) 115758, <https://doi.org/10.1016/j.microrel.2025.115758>
36. A. H. Kacha *et al.*, Effects of the Ga_N layers and the annealing on the electrical properties in the Schottky diodes based on nitrated GaAs, *Superlattices Microstruct.* **83** (2015) 827, <https://doi.org/10.1016/j.spmi.2015.04.017>
37. A. Rabehi, M. Amrani, Z. Benamara, B. Akkal, and A. H. Kacha, Electrical and photoelectrical characteristics of Au/Ga_N/GaAs Schottky diode, *Optik (Stuttg)*, **127** (2016) 6412, <https://doi.org/10.1016/j.ijleo.2016.04.113>
38. A. Rabehi *et al.*, Simulation and Experimental Studies of Illumination Effects on the Current Transport of Nitridated GaAs Schottky Diode, *Semiconductors*, **52** (2018) 1998, <https://doi.org/10.1134/S106378261816025X>
39. Z. Tekeli, Ş. Altı ndal, M. Çakmak, S. Özçelik, D. Çalışkan, and E. Özbay, The behavior of the I-VT characteristics of inhomogeneous (Ni/Au)-Al_{0.3}Ga_{0.7}N/Al_N/Ga_N heterostructures at high temperatures, *J Appl Phys*, **102** (2007) <https://doi.org/10.1063/1.2777881>
40. Z. Tekeli, Ş. Altı ndal, M. Çakmak, S. Özçelik, and E. Özbay, The profile of temperature and voltage dependent series resistance and the interface states in (Ni/Au)/Al_{0.3}Ga_{0.7}N/Al_N/Ga_N heterostructures, *Microelectron Eng.* **85** (2008) 2316, <https://doi.org/10.1016/j.mee.2008.08.005>
41. S. M. Sze, *Semiconductor Devices: Physics and Technology*, vol. 2016.
42. H. Altıntaş, and S. Özcelik, The analysis of leakage current in MIS Au/SiO₂/n- GaAs at room temperature. *Semiconductors*, **47** (2013) 1308,
43. S. M. Sze and K. K. Ng, *Physics of Semiconductor Devices*, Third edition (Wiley-Interscience, Hoboken, NJ, 2007).
44. H. B. Khaless *et al.* Effect of the Ultra-thin Ga_N Interlayer on the Mechanisms of Conduction in Au/GaAs Schottky Barrier Diodes. *Semiconductors* **59** (2025) 551-560, <https://doi.org/10.1134/S1063782624602589>
45. A. Wang, L. Zeng, and W. Wang, Simulation of gate leakage current of AlGa_N/Ga_N HEMTs: Effects of the gate edges and self-heating. *ECS Journal of Solid State Science and Technology*, **6** (2017) S3025.